Hindawi
Mathematical Problems in Engineering
Volume 2022, Article ID 4140905, 10 pages
https://doi.org/10.1155/2022/4140905

Research Article

The Statistical Analysis of Anomalous Anticyclone in Ocean Atmosphere and Economy Based on Target Tracking Algorithm

Min Wan[1,2] **and Mishal Sohail**[3]

[1]*School of Statistics, Jiangxi University of Finance and Economics, Jiangxi Provinces, Nanchang 333000, China*
[2]*Nanchang Jiaotong University, Jiangxi Provinces, Nanchang 330100, China*
[3]*Department of Industrial Engineering, International Ataturk Alatoo University, Bishkek, Kyrgyzstan*

Correspondence should be addressed to Mishal Sohail; dr.mishalsohail@mail.cu.edu.kg

Received 7 May 2022; Revised 8 June 2022; Accepted 14 June 2022; Published 6 July 2022

Academic Editor: Naeem Jan

Based on the importance of climate change in the environmental and economic fields, this study analyzes the impact of climate change on the economy based on the current situation, including the impact on sensitive industries and the impact on each district, in order to study the impact of abnormal atmospheric anticyclones on the economy. Furthermore, this study enhances the image-tracking algorithm, fuses the registered radar picture using the wavelet multiresolution analysis approach, and decomposes the registered radar image using the Mallat algorithm to retrieve the low- and high-frequency components of the image. Because the information included in the frequency components after wavelet decomposition differs, this study uses appropriate fusion algorithms for the decomposed low-frequency and high-frequency components, respectively, to produce panoramic photographs with acceptable visual effects. Through experimental research, it can be seen that the statistical analysis model of anomalous anticyclone in ocean atmosphere and economy based on the target tracking algorithm proposed in this study has a good simulation operation effect, and it also verifies that there is a certain correlation between the atmospheric anomalous anticyclone and the economy.

1. Introduction

In recent decades, the global temperature has generally risen, the greenhouse effect has become an indisputable fact in the world, and the issue of climate change has also become a hot issue of concern to the world. As people continue to deepen their understanding of the relationship between human production activities and global climate change, the international community is also constantly strengthening research on climate-change issues. In March 2014, the IPCC issued the fifth assessment report on climate change. In September of the same year, the United Nations Climate Change Summit was held. The United Nations Climate Change Conference concluded a historic "Paris Agreement" in December 2015. Climate change has become a significant international concern impacting global development, affecting many elements of human social and economic growth. Global climate change has already had and will continue to have its impacts and adjustments. We will confront some degree of climate change in the future, even if the most hopeful strategy for decreasing greenhouse gas emissions is implemented. Furthermore, the effects of climate change are already being felt in Europe and across the world, and these effects and changes will outstrip society's existing reaction capability [1]. Furthermore, governments in various countries have increasingly recognized that climate-change factors must be considered in order to maintain the economy's and society's stability and rapid development, and coping with climate change has become a basic consideration in policy planning in economic development [2]. Therefore, addressing climate change has become an urgent task facing the world, and mitigation and adaptation are the two major aspects of the response. Among them, mitigation is long-term and arduous, while adaptation

is more realistic and urgent. In the short term, adaptation can reduce the risk of climate change and enhance the ability to adapt. In the long term, adaptation can promote the sustainable development of the economy and society. As climate-change mitigation actions cannot be effective for a while, under such circumstances, we need to adopt more targeted adaptation strategies and countermeasures, which have become a more urgent and important choice for all countries.

Climate change is not only a typical global environmental issue but also a development issue. For example, climate change has brought major impacts and severe challenges to China's climate, environment, and development. Therefore, adapting to climate change is a long-term task, and adaptation countermeasures and actions need to comprehensively consider a variety of factors, such as socioeconomic conditions, development plans, and local environment. Therefore, it is necessary to study economic development issues in the context of climate change based on the actual situation in the region, and to study climate change-related countermeasures from the standpoint and perspective of adaptation, promote the development and improvement of adaptation countermeasures, and improve adaptability. This can not only provide solutions to the climate-change constraints of economic development but also provide a certain strategic development direction for the long-term sustainable development of our country's economy in the long run, which has important academic and practical significance [3].

More and more countries, organizations, and the public are beginning to pay attention to climate change and respond to climate change. The most notable one is the concern about global warming and carbon dioxide emissions, which has become a key issue for scholars in various fields.

This study combines the image target tracking algorithm to analyze the correlation between abnormal anticyclones in the ocean and the atmosphere and economic development. This method can not only effectively improve the efficiency of economic development, but also increase the risk of coping with disasters and improve social stability.

2. Related Work

The warming impact of greenhouse gases was conceptually acknowledged in the literature [4]. The particular influence of greenhouse gases on temperature variations was explained in the literature [5]. According to the research [6] when carbon dioxide concentrations double, the global average temperature increases. Many scientists progressively concluded that man-made greenhouse gas emissions had an impact on climate change, which paved the way for human climate research and gave rise to the field of "climate change economy." The "Pigouvian tax" hypothesis of internalizing external costs was presented in the literature [7], establishing the groundwork for environmental economic theories and initiatives. The literature [8] issued an economic study on climate change from the standpoint of economic losses and expenses, urging the world to adopt effective legislative actions to prevent climate change as soon as feasible. The scientific foundation, effect, adaptability, susceptibility, and danger of climate change, and technology and policy approaches for mitigating and adapting to climate change, were all examined in detail in the literature [9]. It gives other areas, disciplines, specialists, and researchers greater information and expertise to investigate climate-change adaptation and policy.

The Paris Agreement reached in 2015 not only includes decisions such as nationally determined contributions and strengthened actions before 2020, but also includes goals, mitigation, adaptation, funding, inventory mechanisms, and technologies, which also points out the direction for future cooperation among countries around the world to address climate change, and marks the starting point of a new global climate order [10]. In addition, there are more experts and scholars studying climate-change issues, the impact of climate change on various industries, and how to deal with climate change from the perspective of economics. The literature [11] studied the impact of climate change on tourism in the Caribbean through empirical analysis and pioneered that climate change has had an adverse impact on coastal tourism by causing sea level rise. The literature [12] analyzed the impact of meteorological factors on the output value of various industries in the United States, and explained the relationship between meteorological factors and the US economy. The literature [13] used the Ricardian model to study the effects of regional temperature and precipitation on crop yields, and concluded that crop yields are more sensitive to temperature changes, the temperature has a positive impact on farmers' income, and precipitation has a negative impact. The literature [14] used the production function economic model to also assess the impact of climate change on crop yields. The literature [15] analyzed the progress of developed countries in promoting adaptation to climate change. The literature [16] illustrated the need for economic policies to solve the funding problem for climate-change adaptation. The literature [17] analyzed European countries' climate policy decisions from multiple fields. The literature [18] combined socioeconomic scenarios and adaptation plans to quantitatively analyze the current and future flood risks of coastal cities, and infer the economic losses that may be suffered due to floods.

The literature [19] clearly pointed out that one of the essences of carbon emission reduction problems caused by climate change is economic problems, because emission reduction must pay economic costs. The literature [20] used mathematical models and related analytical methods to quantitatively assess the vulnerability of agricultural floods in southern Hunan. The literature [21] divided the vulnerable areas of the water resource system by establishing vulnerability evaluation indicators, and summarizes the vulnerability of water resources and the response to climate change. The literature [22] constructed a new economic-climate model to evaluate the impact of climate change on food production. The conclusions obtained are basically in line with the research results of agricultural meteorology and the actual situation of the agricultural economy.

3. Harris Feature Point Matching

After the Harris feature points are extracted, they need to be matched to eliminate the matching points that do not meet the requirements. The matching process of feature points contains two key strategies: similarity measurement and search strategy.

The similarity measurement is used to describe the correlation between the reference image and the feature point set of the image to be spliced, and a good measurement criterion is effective for image registration. Image matching algorithms based on feature points usually use various distance functions as measurement criteria for matching. This section intends to coarsely match the Harris feature points of the radar image through the improved Euclidean distance.

The search strategy refers to the method of finding the best match between the images to be spliced in the feature space through the selected similarity criterion. This is of great significance for reducing the calculation time of the matching process. A suitable search strategy is chosen to optimize the matching algorithm based on the features of the pictures to be spliced and the performance metrics necessary for matching. In this study, the Harris feature points for matching are derived from the contour of the radar picture. In comparison to the original picture, the number of feature points has been drastically decreased, and the image is much more accurate. As a consequence, the feature point matching employs a reasonably simple exhaustive search technique, the computation amount is not greatly increased, and the matching result is satisfactory.

We assume that the feature points in the reference image and the image to be stitched are a and b, and the descriptors of a and b are D_a and D_b, respectively. The Euclidean distance is defined as follows:

$$di\ st = \sqrt{\sum_{i=1}^{H} \left(D_a(i) - D_b(i)\right)^2}. \quad (1)$$

Compared with the traditional Euclidean distance matching algorithm, this study adopts an improved Euclidean distance judgment criterion. In this study, the ratio of the Euclidean distance between the closest feature point and the second adjacent feature point of the feature point extracted from the reference image and the feature point extracted from the image to be stitched is used as the matching decision criterion. If the ratio is greater than the threshold set in advance, the two feature points are considered to meet the requirements and are output as matching feature points. In this study, the threshold value is selected as 0.8, and the matching process is shown in Figure 1.

The result of Harris feature point matching based on improved Euclidean distance matching is shown in Figure 2. It can be seen from the figure that most of the matching results are good, and there are only a few mismatched points.

In the process of matching picture feature points, there are inevitable mismatches owing to image quality issues or the limits of similarity measuring methodologies.

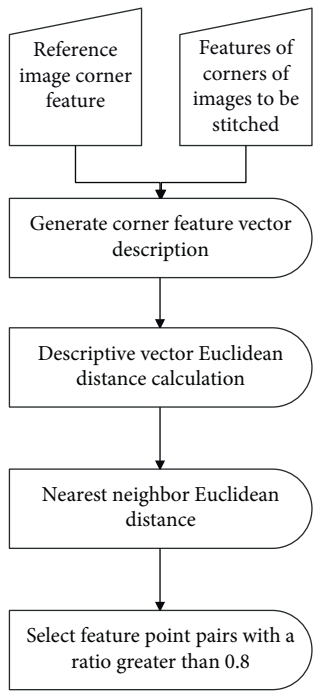

Figure 1: Harris feature point matching process.

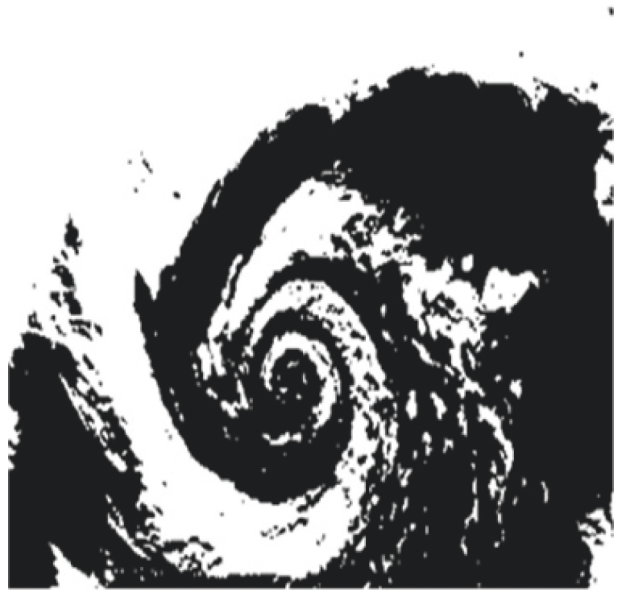

Figure 2: Harris feature point matching results.

Mismatching will result in erroneous coordinate transformation connections between spliced pictures, perhaps causing the whole process to fail. This issue is well solved by the random sampling consensus method.

Although the extraction of the respective feature point sets is utilized to remove the erroneous matching points after extracting the contour feature points and Harris feature points of the stitched picture, the experimental findings show that mismatching still persists to some extent. Because of its robust approach and excellent accuracy, the RANSAC

algorithm is commonly employed in picture stitching to minimize mismatches. The feature points that can be correctly matched are called "inner points," and the feature points that deviate far from the normal range or the feature points that introduce noise are called "outer points." The main task of the RANSAC algorithm is to identify the many feature points, find a straight line so that this straight line can fit all the feature points well, that is, the feature points on and near the straight line are the most, and use the feature points on the straight line to estimate the parameter transformation model between the two images to be spliced.

The RANSAC algorithm model fitting is shown in Figure 3. The left of the figure is the original feature point set, and the straight line shown on the right is the best model obtained by the RANSAC fitting of the original feature point set. The blue marked point on the fitted line is the "inner point," and the red marked point outside the line is the "outer point."

The RANSAC algorithm is a hypothesis validation estimation method, so the first key problem it faces is the estimation of the number of random sampling k. We suppose that the probability of randomly selecting a sample of size n, that is, all "inside points" from N feature points, is P. Then, $P(I)$ is as follows:

$$p(I) = \frac{\binom{I}{n}}{\binom{N}{n}} = \prod_{j=0}^{n-1} \frac{I-j}{N-j} \leq \varepsilon^n. \tag{2}$$

In formula (2), ε is the ratio of "inner points" in the feature point concentration, and I is the number of "inner points". If it is assumed that the probability of extracting at least one n pairs of matching points without "outside points" is PT, then the probability of extracting a sample that does not meet the condition, that is, $\eta = 1 - p_T$. Then, the random sampling number k is calculated as follows:

$$\eta = (1 - p(I_k))^k. \tag{3}$$

If η is less than or equal to the threshold η_0, then

$$\begin{aligned} \eta &= (1 - p(I_k))^k \leq \eta_0, \\ k_{\eta_0} &\leq \frac{\ln(\eta_0)}{\ln(1 - p(I_k))} \leq \frac{\ln(\eta_0)}{\ln(1 - \varepsilon^n)}. \end{aligned} \tag{4}$$

Figure 4 depicts the RANSAC algorithm stages in detail. This study employs perspective transformation, necessitating the employment of four pairs of matching points. First, the algorithm picks four pairs of matching points as "inner points" from all feature points and calculates the distance between other points and the straight line formed by these four pairs of matching points. The threshold t is established by the algorithm, and the value used in this study is 0.001. The algorithm adds feature points less than the threshold t to the set of interior points, repeats k times, and selects the set with the largest number of interior points as the best purification result.

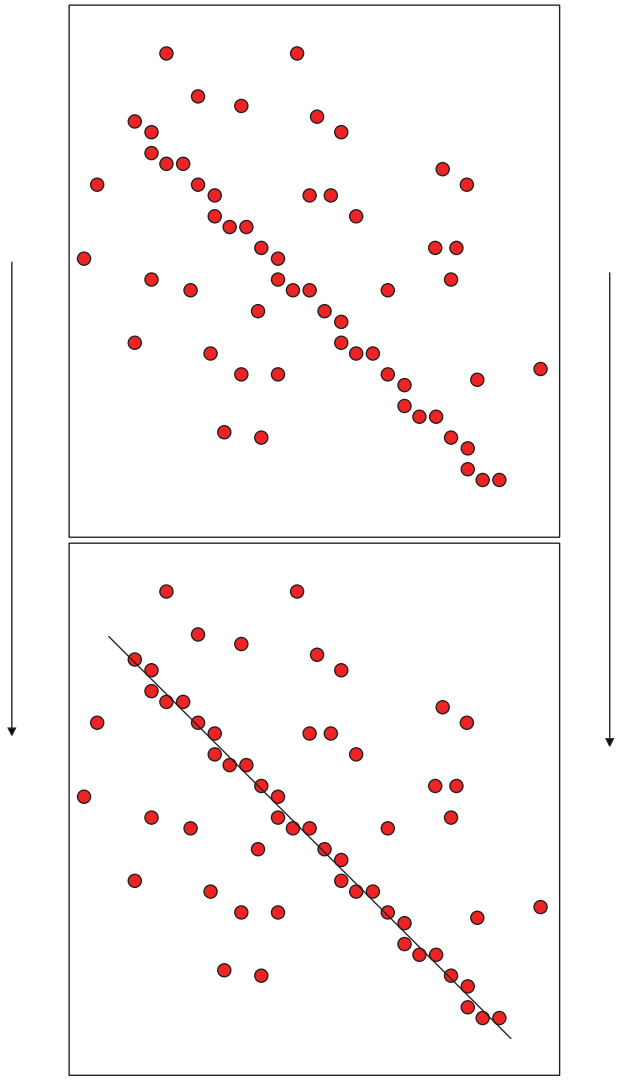

Figure 3: RANSAC algorithm model fitting.

There are different degrees of mismatch between the feature point set obtained by the closed contour matching of the radar image and the Harris feature point set obtained by the Euclidean distance rough matching. We merge the above two sets into a comprehensive feature point set for precise purification of the RANSAC algorithm. The experimental results are shown in Figure 5.

It can be seen from Figures 5 and 6 that mismatching is effectively suppressed, image matching has achieved good results, the number of matching points is significantly reduced, and the operating efficiency is greatly improved.

The normalized projection transformation matrix H obtained by the above two radar images to be spliced through the RANSAC algorithm is shown below as follows:

$$H = \begin{pmatrix} 1.0157 & 0.0032 & -118.1537 \\ -0.0095 & 0.9955 & 0.2673 \\ -0.0002 & 0.0000 & 1.0000 \end{pmatrix}. \tag{5}$$

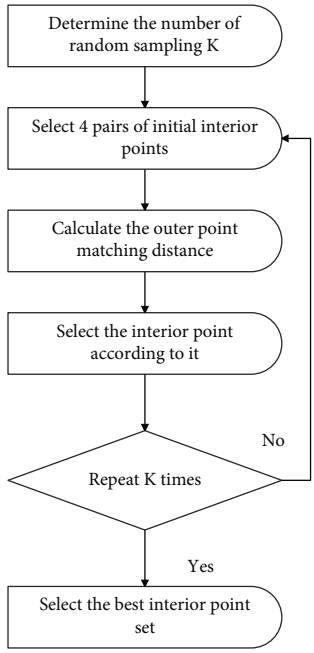

Figure 4: RANSAC algorithm flow.

Figure 5: Matching results of comprehensive feature point set.

The experiment sets the scale factor of the two radar images to be spliced $s = 1$ and the angle rotation factor $\theta = 0$; then, the theoretical value of the image projection transformation matrix is as follows:

$$H_{\text{true}} = \begin{pmatrix} h_1 = s \times \cos\theta = 1 & h_2 = s \times \sin\theta = 0 & h_3 \\ h_4 = s \times \cos\theta = 0 & h_5 = s \times \cos\theta = 1 & h_6 \\ h_7 & h_8 & 1 \end{pmatrix}. \tag{6}$$

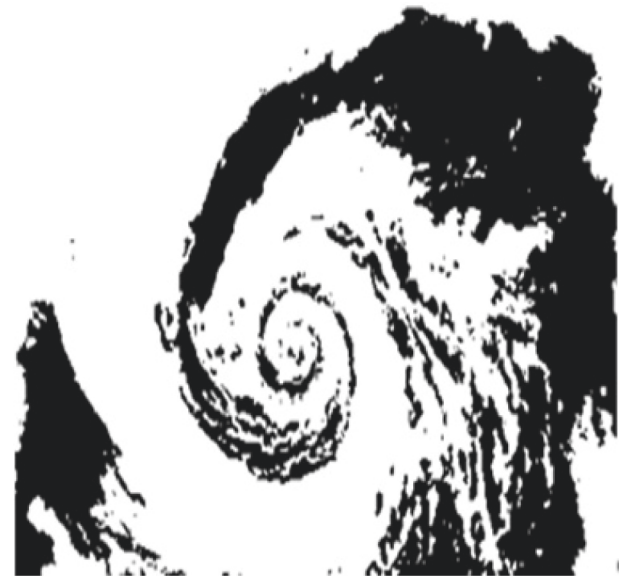

Figure 6: RANSAC exact matching result.

The scale factor is $s = 1.015$, the error is 0.015, the angle rotation factor is $\theta = 0.181$, and the angle error is 0.181 degrees, as determined by comparing the abovementioned projection transformation matrix H with the theoretical value He. It can be shown that the matching precision approaches subpixel levels and fulfills the radar image stitching criteria.

The lens of the camera and the portion or all of the scene to be studied help explain the concept of multiresolution analysis. When the scale factor an is increased, it is analogous to zooming in on the camera's focal length, allowing us to capture the full scene. When the scale factor an is lowered, the focal length of the camera is shortened, and we can catch the scene's delicate local details. The core of the multiresolution analysis is this sort of step-by-step objective from rough to fine and from far to close.

The basic idea of the Mallat pyramid algorithm can be summarized as follows.

The object of this study is the Doppler radar image, and the image is a two-dimensional matrix, so we need to expand the wavelet to two-dimensional space when we study radar image. Similarly, multiresolution analysis also needs to be extended from one-dimensional to two-dimensional space $L^2(R^2)$. The two-dimensional Mallat algorithm is briefly described as follows.

If V_j is a series of closed subspaces satisfying multiresolution analysis in $L^2(R)$, then V_j^2 is the generalization of two-dimensional space (RS). If it is assumed that the two-dimensional signal analyzed is $f(x, y) \in V_j^2$, then the two-dimensional Mallat decomposition algorithm can be obtained as follows:

$$f(x, y) = A_{j+1} f + D_{j+1}^1 f + D_{j=1}^2 f + D_{j+1}^3 f. \tag{7}$$

Among them, the first-level two-dimensional Doppler radar image is composed of four parts after wavelet transformation as follows:

$$\begin{cases} A_{j+1}f = \sum_{m1,m2\in Z} C_{j+1;m1,m2\phi j+1;m1,m2}, \\ D^{i}_{j+1}f = \sum_{m1,m2\in Z} D^{i}_{j+1;m1,m2\psi j+1;m1,m2}\ (i = 1, 2, 3). \end{cases} \tag{8}$$

$$\begin{cases} C_{j+1}f = \sum_{k1,k2\in Z} h_{k1-2m1}h_{k2-2m2}C_{j:\ k1,k2}, \\ D^{1}_{j+1}f = \sum_{k1,k2\in Z} h_{k1-2m1}g_{k2-2m2}C_{j:\ k1,k2}, \\ D^{2}_{j+1}f = \sum_{k1,k2\in Z} h_{k1-2m1}g_{k2-2m2}C_{j:\ k1,k2}, \\ D^{1}_{j+1}f = \sum_{k1,k2\in Z} h_{k1-2m1}g_{k2-2m2}C_{j:\ k1,k2}. \end{cases} \tag{9}$$

$$\begin{bmatrix} c^{j}_{k,m} & d^{j,1}_{k,m} \\ d^{j,2}_{k,m} & d^{j,3}_{k,m} \end{bmatrix}. \tag{10}$$

As shown in equation (10), the wavelet coefficients obtained from the radar image after wavelet transformation correspond to LL, HL, LH, and HH, respectively. LL stands for low-frequency components, and it keeps the majority of the information from the original picture, which is an approximate representation. High-frequency components, such as edges and area contours, are represented by the letters HL, LH, and HH. A low-pass filter and a high-pass filter are combined to create each component's information. The low-frequency component LL may be decomposed at the following level if the first-level breakdown does not fulfill the predefined parameters. The Mallat algorithm, on the other hand, does not decompose the impact; the more layers, the better. It must be examined in light of unique issues. The quantity of computation will grow dramatically if there are too many decomposed layers, and the picture processing result will not be greatly enhanced.

According to the idea of wavelet multiresolution analysis and the Mallat algorithm, for two-dimensional images, wavelet multiresolution analysis has good local characteristics and multiscale characteristics in both the space domain and the frequency domain. After the wavelet decomposition of the Doppler radar image, we can intuitively understand the information of each frequency band component after the radar image is decomposed, and provide a specific theoretical basis for the radar image fusion method and rule below.

The wavelet decomposition of the radar image is shown in Figure 7.

In this study, a method based on wavelet multiresolution analysis is used to fuse the registered radar images. The wavelet multiresolution analysis method has been described in the previous section. The registered radar image is decomposed by the Mallat algorithm to obtain the low-frequency and high-frequency components of the image. Since the information contained in the frequency components after wavelet decomposition is different, if the frequency components are not distinguished, a single fusion rule is adopted. The final fusion effect will be greatly reduced, so this study adopts respective suitable fusion strategies for the decomposed low-frequency components and high-frequency components, and a panoramic image with good visual effects can be obtained.

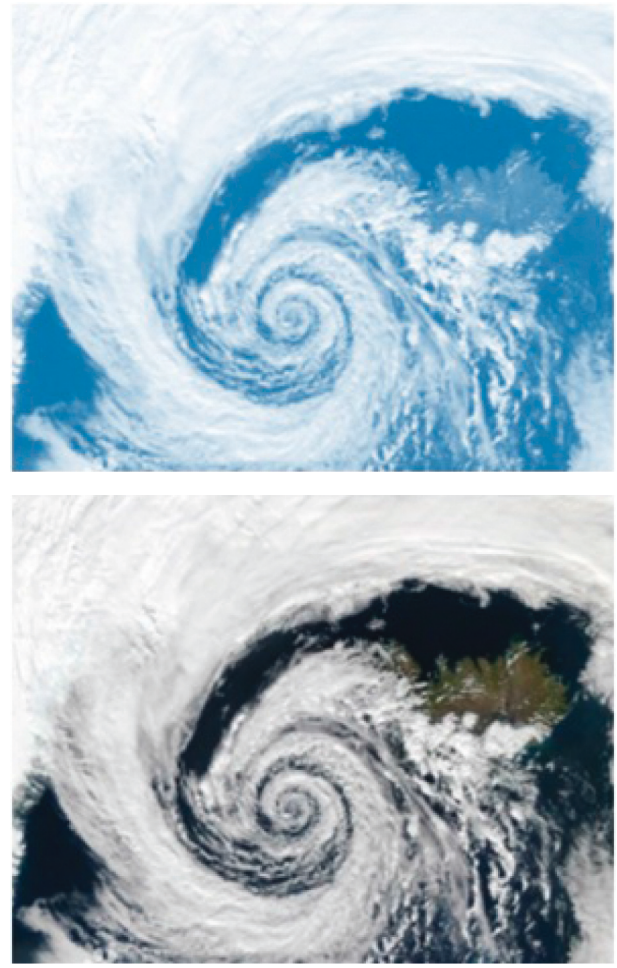

Figure 7: First-level wavelet decomposition of the original image.

Wavelet multiresolution analysis may be used to fuse radar pictures and provide decent results; however, the wavelet decomposition level must be modest. In general, the transition region of image fusion will be smoother and the visual impact will be greater when there are more levels of decomposition, but when the number of layers of picture decomposition is too high, the image information will be lost and the fusion effect will not be proportionate. The improvement, and the quantity of computation required, is too big and time-consuming. Therefore, when choosing the number of decomposition layers, comprehensive consideration should be made according to the type of image to be processed. In this study, the number of wavelet decomposition layers is selected as three layers, which can already ideally fulfill the predetermined requirements.

After the registered radar image is decomposed by Mallat, it is necessary to select an appropriate fusion strategy for each frequency component. The selection of the fusion strategy is a key step for the final fusion of the radar image. The radar image fusion process is shown in Figure 8.

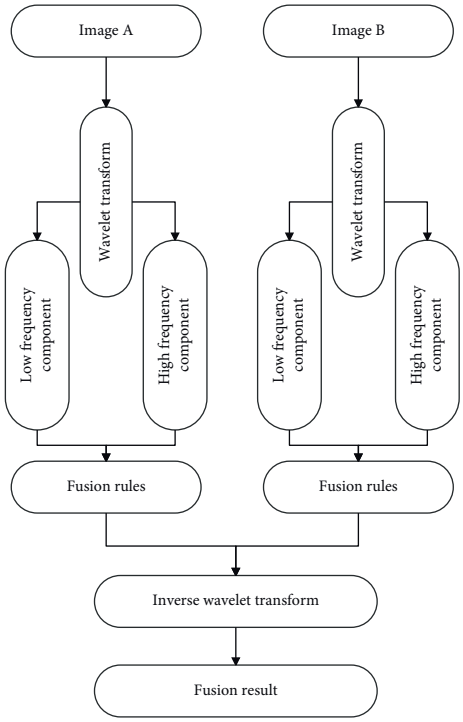

Figure 8: Radar image fusion based on wavelet transform.

The fusion rule of the low-frequency domain in this study adopts the weighted average fusion method. The weighted average fusion method is similar to the average value method. However, in the overlapping area, the low-frequency coefficients are not simply superimposed, but are weighted and then averaged. The weighted average method is simple and intuitive, has a small amount of calculation, and maximizes the use of the pixel value information of the image. If $f_N^A(x, y)$ and $f_N^B R(x, y)$ are the low-frequency coefficients of the two images, respectively, then there are the following:

$$f_N^F(x, y) = \begin{cases} f_N^A(x, y) & (x, y) \in I_1, \\ w_1(x, y) f_N^A(x, y) & \\ \quad + w_2(x, y) f_N^B(x, y) & (x, y) \in (I_1 \cap I_2), \\ f_N^B(x, y) & (x, y) \in I_2. \end{cases} \tag{11}$$

w_1 and w_2 represent corresponding weights and satisfy $w_1 + w_2 = 1, 0 < w_1 < 1, 0 < w_2 < 1$. The selection of weight coefficients w_1 and w_2 is very important for the weighted average fusion algorithm. If the horizontal boundary coordinates of the overlapping parts of the two radar images to be stitched are $x_{\max}$ and $x_{\min}$, and the vertical boundary coordinates are $y_{\max}$ and $y_{\min}$, the weight coefficients are defined as follows:

$$w_1 = \frac{(x_{\max} - x)}{(x_{\max} - x_{\min})} w_2 = 1 - w_1. \tag{12}$$

The fusion rule of the high-frequency domain in this study adopts a window-based method to take the absolute value of the coefficient. First, the absolute value of the high-frequency coefficient of the two radar images to be spliced is compared, and the larger one is selected as the final result. If $g_i^A(x, y)$ and $g_i^B(x, y)$ are the high-frequency coefficients of the two figures, respectively, then there are the following:

$$g_i^F(x, y) = \begin{cases} g_i^A(x, y) \left| g_i^A(x, y) \right| > \left| g_i^B(x, y) \right|, \\ g_i^B(x, y) \left| g_i^A(x, y) \right| < \left| g_i^B(x, y) \right|. \end{cases} \tag{13}$$

The final result calculated by the above formula will be verified for window consistency. If it is assumed that the high-frequency coefficients in the center of the window are fused from the reference image $g(x, y)$ and the coefficients in the window neighborhood (3×3 or 5×5 windows) are taken from the image $g_i^B(x, y)$ to be spliced, then the fusion coefficient is changed to $g_i^B(x, y)$ and vice versa. The abovementioned image high-frequency coefficient fusion method increases the correlation between a single pixel and the surrounding neighborhood, the fusion effect is more comprehensive, and it has a wide range of applicability.

4. Statistical Analysis of Abnormal Anticyclones in Ocean Atmosphere and Economy Based on Target Tracking Algorithm

The target tracking approach is used in this research to do a statistical analysis of aberrant anticyclones in the ocean atmosphere and economy. The aberrant anticyclones of the ocean and atmosphere in past years are listed on this page. The data are taken from the Bureau of Meteorology's website, and a correlational study is carried out between aberrant anticyclones in the ocean atmosphere and the agricultural economy with the greatest association with the weather. The statistical yearbook is where the agricultural research data originate from. Table 1 shows the definitions of model variables and descriptive statistics.

This study uses panel data with cross section and time series to perform regression analysis. In order to further reduce the adverse effects of cross-sectional heteroscedasticity and time-series autocorrelation on regression, this study uses the panel generalized least squares estimation method to determine whether to choose a fixed-effects model or a mixed-effects model. In the end, this study draws the conclusion that the mixed-effects model is better than the fixed-effects model and uses period weighting to estimate on this basis. Table 2 shows the regression results of the final mixed-effects model.

From the above research, it can be seen that the statistical analysis model of anomalous anticyclone in ocean atmosphere and economy based on the target tracking algorithm proposed in this study has a good simulation operation effect, and it also verifies that there is a certain correlation between anomalous anticyclone in ocean atmosphere and economy.

Table 1: Model variable definitions and descriptive statistics.

Variable name	Variable definitions	Average value	Standard deviation	Maximum value	Minimum value
Y rice yield	Total rice output (ten thousand tons)	624.968	707.146	2581.944	0.131
A sown area of rice	Rice sown area (thousand hectares)	930.582	1008.894	3361.613	0.202
M agricultural machinery	Total power of agricultural machinery used for rice production (10,000 kilowatts)	431.316	496.278	2798.658	0.173
F fertilizer input	Converted amount of agricultural chemical fertilizer put into rice production (ten thousand tons)	31.937	34.180	104.355	0.010
L labor force	Number of agricultural laborers invested in rice production (10,000 people)	84.878	94.957	323.921	0.017
I effective irrigation area	Effective irrigation area of rice (thousand hectares)	319.323	354.809	1210.205	0.148
T temperature	Monthly average temperature of rice growing period (°C)	20.794	3.507	28.129	13.260
P precipitation	Average monthly precipitation during rice growing period (mm)	101.781	57.836	301.321	8.504
TE technology advancement	Replace technological progress with time trends	4.534	2.318	8.000	1.000
Area variable D1	East China	0.144	0.355	1.000	≤0.001
Area variable D2	East China	0.181	0.389	1.000	≤0.001
Area variable D3	East China	0.109	0.314	1.000	≤0.001
Area variable D4	Southwest region	0.144	0.355	1.000	≤0.001
Area variable D5	Northwest region	0.140	0.350	1.000	≤0.001
Area variable D6	Northeast area	0.109	0.314	1.000	≤0.001

Table 2: The regression analysis of the mixed-effects model.

Variable	Coefficient	std. error	t-statistic	prob.
Sown area (LNA)	1.848	0.612	3.051	0.003
Mechanical input (LNM)	2.109	0.484	4.399	≤0.001
Fertilizer input (LNF)	−1.428	0.785	−1.837	0.072
Labor force input (LNL)	−1.661	0.418	−4.012	≤0.001
Effective irrigation area (LNI)	0.611	0.617	1.000	0.327
Quadratic term of sown area ((LNA)2)	−0.027	0.283	−0.097	0.933
Quadratic term of mechanical input ((LNM) 2)	0.245	0.161	1.540	0.130
Quadratic term of fertilizer input ((LNF) 2)	−0.581	0.256	−2.300	0.024
Quadratic term of labor input ((LNL)2)	−0.386	0.136	−2.845	0.005
Quadratic term of effective irrigation area ((LNI) 2)	−0.883	0.238	−3.746	≤0.001
Sown area and mechanical input (LNA × LNM)	−0.952	0.192	−5.003	≤0.001
Sown area and fertilizer input (LNA × LNF)	−0.349	0.176	−2.004	0.049
Sown area and labor input (LNA × LNL)	0.724	0.167	4.398	≤0.001
Sown area and effective irrigation area (LNA × LNI)	0.515	0.280	1.859	0.068
Machinery and fertilizer input (LNM × LNF)	0.447	0.132	3.413	0.001
Machinery and labor force input (LNM × LNL)	0.070	0.112	0.624	0.543
Machinery and effective irrigation area (LNM × LNI)	0.177	0.120	1.480	0.146
Fertilizer and labor input (LNF × LNL)	0.066	0.112	0.589	0.567
Fertilizer and effective irrigation area (LNF × LNI)	0.524	0.140	3.773	≤0.001
Labor force and effective irrigation area (LNL × LNI)	−0.405	0.150	−2.713	0.008
Temperature change (LNT)	−4.297	0.924	−4.695	≤0.001
Quadratic term of temperature change ((LNT)2)	1.164	0.348	3.371	0.001
Precipitation change (LNP)	0.278	0.149	1.881	0.065
Quadratic term of precipitation change ((LNP)2))	−0.068	0.034	−2.017	0.047
Technological progress (TE)	2.655	0.313	8.557	≤0.001
Quadratic term of technological progress (TE2)	−1.663	0.303	−5.552	≤0.001
East China (D1)	0.112	0.052	2.213	0.030
North China (D2)	−0.206	0.068	−3.065	0.003
Central China (D3)	0.213	0.040	5.370	≤0.001
Southwest region (D4)	0.193	0.080	2.442	0.017
Northwest region (D5)	0.319	0.073	4.416	≤0.001
Northeast China (D6)	0.036	0.076	0.481	0.641
R2	0.999			
Adjust R2	0.999			

5. Conclusions

This study analyzes the impact of climate change on the economy based on actual conditions, including the impact on sensitive industries and the impact on each district, and provides countermeasures and suggestions for adapting to climate change, based on the importance of climate change in the environmental and economic fields. Furthermore, the image target tracking technique is used in this work to investigate the relationship between the anomalous anticyclone in the ocean atmosphere and economic growth. This strategy can not only raise the risk of catastrophes and promote social stability, but it can also improve the efficiency of economic growth.

In the context of climate change, based on panel data from various provinces across the country, this study first uses descriptive statistics to analyze the characteristics of climate change and China's agricultural development. Second, this study uses the panel data model to simulate the data, analyze the impact of climate change on our country's total agricultural output and its contribution rate, and simulate the impact of future climate change on the total agricultural output through various climate-change scenarios. The research shows that the statistical analysis model of anomalous anticyclone in ocean atmosphere and economy based on the target tracking algorithm proposed in this study has a good simulation operation effect, and also verifies that there is a certain correlation between atmospheric anomalous anticyclones and economy.

Data Availability

The data used to support the findings of this study are available from the author upon request.

Conflicts of Interest

The authors declare that they have no conflicts of interest.

References

[1] J. Pipek and S. Nagy, "An economic prediction of refinement coefficients in wavelet-based adaptive methods for electron structure calculations," *Journal of Computational Chemistry*, vol. 34, no. 6, pp. 460–465, 2013.

[2] S. Nagy and J. Pipek, "An economic prediction of the finer resolution level wavelet coefficients in electronic structure

calculations," *Physical Chemistry Chemical Physics*, vol. 17, no. 47, pp. 31558–31565, 2015.

[3] W. Yu and W Huafeng, "Quantitative analysis of regional economic indicators prediction based on grey relevance degree and fuzzy mathematical model[J]," *Journal of Intelligent and Fuzzy Systems*, vol. 37, no. 2, pp. 1–14, 2019.

[4] P. Karanikić, I. Mladenović, M. S. Sokolov, and M. Alizamir, "Retraction Note: prediction of economic growth by extreme learning approach based on science and technology transfer," *Quality & Quantity*, vol. 53, no. 2, pp. 1095-1096, 2019.

[5] K. Ataka, "Prediction of election result and economic indicator," *resuscitation*, vol. 96, no. 6, p. 84, 2014.

[6] S. Barde, "Back to the future: economic self-organisation and maximum entropy prediction," *Computational Economics*, vol. 45, no. 2, pp. 337–358, 2015.

[7] A. Ferramosca, D. Limon, and E. F. Camacho, "Economic MPC for a changing economic criterion for linear systems," *IEEE Transactions on Automatic Control*, vol. 59, no. 10, pp. 2657–2667, 2014.

[8] L. Zhou, K. K Lai, and J. Yen, "Bankruptcy prediction using SVM models with a new approach to combine features selection and parameter optimisation[J]," *International Journal of Systems Science*, vol. 45, no. 1-3, pp. 241–253, 2014.

[9] D. Bhattacharya, J. Mukhoti, and A. Konar, "Learning regularity in an economic time-series for structure prediction," *Applied Soft Computing*, vol. 76, no. 2, pp. 31–44, 2019.

[10] Y. Geng, Z. Wei, H. Zhang, and M. Maimaituerxun, "Analysis and prediction of the coupling coordination relationship between tourism and air environment: yangtze river economic zone in China as example," *Discrete Dynamics in Nature and Society*, vol. 2020, no. 10, pp. 1–15, Article ID 1406978, 2020.

[11] H. L. Vu, K. T. W. Ng, and D. Bolingbroke, "Time-lagged effects of weekly climatic and socio-economic factors on ANN municipal yard waste prediction models," *Waste Management*, vol. 84, no. 2, pp. 129–140, 2019.

[12] C. Teljeur, O. M. Neill, P. Moran, and L. Murphy, "Using prediction intervals from random effects meta-analyses in an economic model[j]," *International Journal of Technology Assessment in Health Care*, vol. 30, no. 01, pp. 44–49, 2014.

[13] P. Rajsic, A. Weersink, A. Navabi, and K. P. Pauls, "Economics of genomic selection: the role of prediction accuracy and relative genotyping costs[J]," *Euphytica*, vol. 210, no. 2, pp. 1–18, 2016.

[14] F. Jahedpari, T. Rahwan, and S. Hashemi, T. P. Michalak, V. M De, J Padget, W. L Woon, Online prediction via continuous artificial prediction markets," *IEEE Intelligent Systems*, vol. 32, no. 1, pp. 61–68, 2017.

[15] V. Daksiya, H. T. Su, Y. H. Chang, and E. Y. M. Lo, "Incorporating socio-economic effects and uncertain rainfall in flood mitigation decision using MCDA," *Natural Hazards*, vol. 87, no. 1, pp. 515–531, 2017.

[16] S. Lahmiri, "A variational mode decompoisition approach for analysis and forecasting of economic and financial time series," *Expert Systems with Applications*, vol. 55, no. 8, pp. 268–273, 2016.

[17] N. Gordini, "A genetic algorithm approach for SMEs bankruptcy prediction: empirical evidence from Italy," *Expert Systems with Applications*, vol. 41, no. 14, pp. 6433–6445, 2014.

[18] A. Ferramosca, A. H. González, H. Limon, and D. Limon, "Offset-free multi-model economic model predictive control for changing economic criterion," *Journal of Process Control*, vol. 54, no. 3, pp. 1–13, 2017.

[19] C. J. A. Jane, "Hybrid model combined grey prediction and autoregressive integrated moving average model for talent prediction[J]," *Journal of Grey System*, vol. 21, no. 2, pp. 91–102, 2018.

[20] A. K. Nassirtoussi, S. Aghabozorgi, T. Y. Wah, and D. C. L. Ngo, "Text mining for market prediction: a systematic review[J]," *Expert Systems with Applications*, vol. 41, no. 16, pp. 7653–7670, 2014.

[21] M. Ellis and P. D. Christofides, "Integrating dynamic economic optimization and model predictive control for optimal operation of nonlinear process systems," *Control Engineering Practice*, vol. 22, no. 1, pp. 242–251, 2014.

[22] L. J. Linarelli, "Luck, justice and systemic financial risk," *Journal of Applied Philosophy*, vol. 34, no. 3, pp. 331–352, 2017.